Ellipsometric characterization of an AISI 304 stainless steel protective coating

J.J. Fuentes-Gallego, E. Blanco, L. Esquivias

Departamento de Física de la Materia Condensada, Universidad de Cádiz, Apartado de Correos 40, 11510 Puerto Real (Cádiz), Spain

Abstract

Thin and very uniform silica–alumina films were deposited by dip-coating onto AISI-304 stainless steel and submitted to different heat treatments. They were prepared by simultaneous ultrasound-assisted hydrolysis and polycondensation of tetraethylorthosilicate and aluminium-sec-butylate or aluminium nitrate in an atmosphere rich in water vapour. The resulting materials were characterised by ellipsometry in order to optimise the process of avoiding porosity which was submitted to molecular probing. This method informs us of the micropore size distribution, using adsorptive different-sized molecules.

The thickness ranges from 60 to 350 nm, depending on the sol processing and heat treatment. In some samples most of the micropores are only sensitive to molecular probe below 0.7 nm diameter. These and other characteristics will be discussed.

Keywords: Coatings; Ellipsometry; Sintering; Steel

1. Introduction

Coating is one of the most important applications of the sol–gel process, because in addition to the usually claimed advantages of sol–gel processing, it presents specific interesting characteristics as opposed to other deposition methods. Thus, contrary to evaporation, sputtering, chemical vapour deposition, etc., it makes possible inorganic coatings from a liquid precursor without paying special attention to the atmosphere surrounding the sample.

Prevention of steel corrosion by sol–gel processing has been tested using different materials as protective coatings such as SiO_2 [1], SiO_2–B_2O_3 [2], mullite [3], ZrO_2 [4,5], MTOS [6], $ZrCeO_2$ [7] and SiO_2–TiO_2, SiO_2–Al_2O_3 [8]. The most usual problems found in deposing thin films on metals by sol–gel processing come mainly from: differences between film and substrate expansion coefficients, oxidation or sensibilization to the metal corrosion, imperfect coatings of the edges and remaining porosity. The last one is probably the genuine cause of less reliability in sol–gel processed coatings. Therefore, the pore size distribution of sintered films must be characterised as well as microporosity evolution during sintering in order to predict and improve final product performance. This information can be obtained by molecular probing ellipsometry [9,10]. This technique is based on the possibility of using a liquid with a known molecule size and refractive index as adsorbate and measuring the change in the refractive index of film matrix/probe molecule system by reflection ellipsometry. A pore volume distribution can be obtained according to the pore which this molecule can fill by using different sized molecules. The results reported in this paper concern the texture of mullite-like amorphous coating on AISI 304 stainless steel prepared by dip-coating as a function of the processing parameters and variables such as precursors and their concentration and heat treatment.

2. Experimental

2.1. Film preparation

The solutions were prepared from tetraethylorthosilicate (TEOS) as the silica precursor, and aluminium tri-sec butoxide (TBA) or $Al(NO_3)_3 9H_2O$ as aluminium sources, mixed in the ratio 3Al:Si. Methylglycol and 2-propanol were used as solvents. The amount of solvent used was 2/3 of the whole weight. Acetic acid and acetyl-acetonate have been used as complexing agents, with a molar ratio of 0.5 and 1 respect to the TBA, respectively. In Table 1 the code of samples and preparation conditions of the three films series are shown.

Table 1
Sol compositions

Sample	Source of Si	Source of Al	Solvent	Complexing agent
S1	TEOS	TBA	2-propanol	acetylacetone
S2	TEOS	TBA	methylglykol	acetic acid
S3	TEOS	$Al(NO_3)_3 9H_2O$	ethanol	–

Table 2
Van der Waals equivalent sphere diameter and refractive indices of probe molecules

Probe molecule	Diameter (Å)	Refractive index
Water (H_2O)	3.28	1.333
Methanol (CH_3OH)	4.72	1.329
Carbon tetrachloride (CCl_4)	6.49	1.460
Cyclohexane (C_6H_{12})	7.36	1.426
1,5,9-cyclododecaterene ($C_{12}H_{18}$)	9.30	1.507

Contrary to samples S1 and S2, no complexing agent was used to obtain the sample S3 since $Al(NO_3)_3 9H_2O$ has a lower reactivity than TBA. The method proposed by Huling and Messing [11,12] was used instead, as it has proved to increase density thus reducing porosity. They used a sol made by dissolving a fresh gel that crystallises in orthorhombic mullite (o-mullite) at 700 °C, being this crystallisation temperature ~ 500 °C lower than those previously reported, thus obtaining gels with a higher molecular-scale chemical homogeneity.

The solutions have been submitted to 20 kHz frequency and 0.12 kJ ultrasonic energy. Transparent and stable solutions are obtained after insonation.

The AISI 304 substrate, previously ultrasonically degreased in trichloroethylene, was polished with SiC of grit 220, 500, 800 and 1200 and 3–1 μm diamond paste before film deposition.

The thin films were made by dipping the substrates in the solutions at a speed of 1.4×10^{-3} m s^{-1}. The samples were dried at 60 °C for 15 min and heat treated at 60, 200, 350, 500 and 675 °C for 12 h with a heating speed of 5 °C min^{-1}.

2.2. Ellipsometry measurements

The measures were obtained by reflection ellipsometry with a PLASMOS SD-2300 automatic ellipsometer with a spot size of 2 mm^2 and a wavelength of 632.8 nm. The ellipsometric angles, Ψ and Δ, are obtained at the same point, at multiple incidence angles (MAI), being correlated with film thickness and refractive index, n, by means of McCrackins routines [13,14] by interactive calculus with software provided by PLASMOS.

The porosity of the films studied has been studied by molecular probe ellipsometry (MPE). The experimental setting is similar to that made by Yeatman et al. [9,10]

except for a vacuum pump being used instead to evacuate the sample chamber. In this technique, the film is placed in a hemispherical sealed chamber on the sample stage of the ellipsometer (Fig. 1); first dry N_2 gas is passed through the chamber pumped out by the vacuum pump to empty the pores, in a 9.7 torr pressure atmosphere, of any condensed adsorbate, until Ψ and Δ values remain steady. Then, N_2 gas previously bubbled through the liquid adsorbate, is passed over the sample to fill the pores; in each case the refractive index is measured, when Ψ and Δ reach a steady value. In the first stage the refractive index grows because the pores are being filled with a liquid of $n > 1$, while the thickness remains constant. When all the accessible pores are completely full, an external layer is formed in the second stage. Then, thickness grows and the refractive index decreases because the refractive index of adsorbate is lower than that of the film.

If it is assumed that all the accessible pores are completely emptied in N_2 dry or totally filled with adsorbate when the atmosphere is saturated, the pore volume and the solid skeleton index can be determined by an extension of the Maxwell–Garnett effective medium expression [15]:

$$\frac{n_f^2 - n_p^2}{n_f^2 - 2n_p^2} = \left(1 - \nu_p\right)\frac{n_s^2 - n_p^2}{n_s^2 - 2n_p^2} \tag{1}$$

where n_f, n_s and n_p are the refractive indices of film, solid skeleton and pores respectively, and ν_p is the adsorbate volume fraction. This expression accounts for the contribution of each component to a composite's refractive index. We have used water, methanol, carbon tetrachloride, cyclohexane and 1,5,9-cyclododecatriene as adsorbates, which sizes range from 3 to 10 Å. Adsorbate molecule size and refractive index are shown in Table 2.
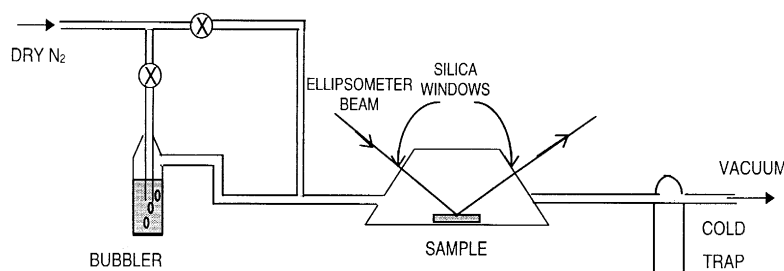
Fig. 1. Experimental device employed in molecular probe ellipsometry (MBE).

3. Results and discussion

Fig. 2(a) and 2(b) show the film thickness and refractive index evolution during heating. As expected, there is a decrease in thickness value for increasing temperature. Two different regimes can be observed for S1 and S2; below 500 °C samples are more sensitive to the temperature increase than above this temperature because of the evolving water and solvents; at temperatures > 500 °C, there is no significant residues escape but film densification takes place by pore collapse due to viscous relaxation, according to the differential thermogravimetric experiments of bulk S1, S2 and S3 gels DTG, presented in Fig. 3. Although processed in the same conditions (concentration, dip coating speed, thermal treatment), the S2 sample is thicker than S1, as a consequence of the different viscosity of the starting sol. However, both films show the same behaviour, reaching the same thickness and refractive index over 500 °C. The S3 sample is the thinnest, mainly due to the minor volume of organic compounds in the starting sol, leading to lower sol viscosity.

The DTG plots represented in Fig. 3 show that the most important weight loss is produced in the 200–350 °C temperature range, corresponding to the evolving organic residues locked in the pores' wall. The weight loss below 200 °C corresponds to the elimination of adsorbed species present in the pores.

The refractive index evolution (Fig. 2(b)) has a different behaviour in the S3 sample. S1 and S2 samples show a
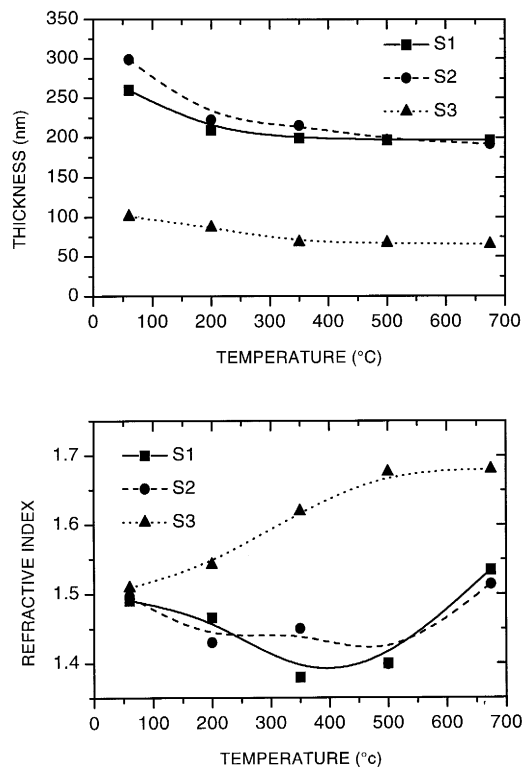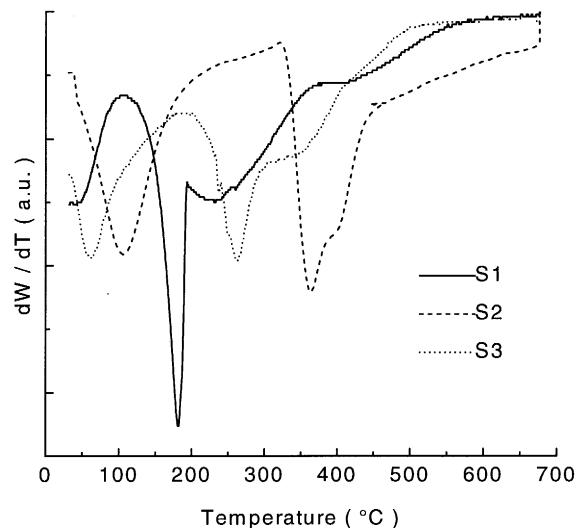
Fig. 3. Derivative thermogravimetric analysis (DTG) of samples S1, S2 and S3. All the experiments were carried out at 5 °C min^{-1}.

minimum once the organics have been removed, increasing at higher temperatures due to the film sintering. Nevertheless, the S3 sample does not behave this way, showing a monotone increase of the refractive index, hence of the density, with increasing temperature. The density of the S3 sample is higher than that of S1 and S2 in the whole of studied range of temperature. This agrees with a higher molecular scale chemical homogeneity of the S3 sample [11,12].

Fig. 4 shows the variation of film thickness throughout the sample. Films present a very constant thickness in most of the surface. In the edges the thickness decrease, as expected by the effect of an imperfect coating produced in this zone. Nevertheless, it is possible to affirm that the film completely covers the steel surface. The film thickness uniformity increases when the sample is heat treated.

The results of the porosity study by MPE of samples S1 and S3 are shown in Fig. 5. The volume fraction porosity, calculated by Eq. (1), is plotted vs. probe molecule size. The distributions present an important decrease in an intermediate range of the measurements interval mostly between 4.5 and 6.5 Å, the porosity fraction values remaining nearly constant out of this range. This general behaviour has suggested that pore volume fraction follows a sigmoidal law as a function of pore diameter. This behaviour is not so evident in the S1 sample heat treated at 675 °C.

The porosity evolution with the heat treatment agrees with the refractive index, thickness and DTG results. The S1 sample presents higher porosity than that of S3 and the maximum porosity appears at 350 °C once all the organics have been removed and the viscous sintering has not yet started. For higher temperatures, a progressive porosity reduction is found due to the pore collapse caused by the film densification. S3 sample sintering starts at a lower

Fig. 2. Thickness and refractive index film evolution with temperature.
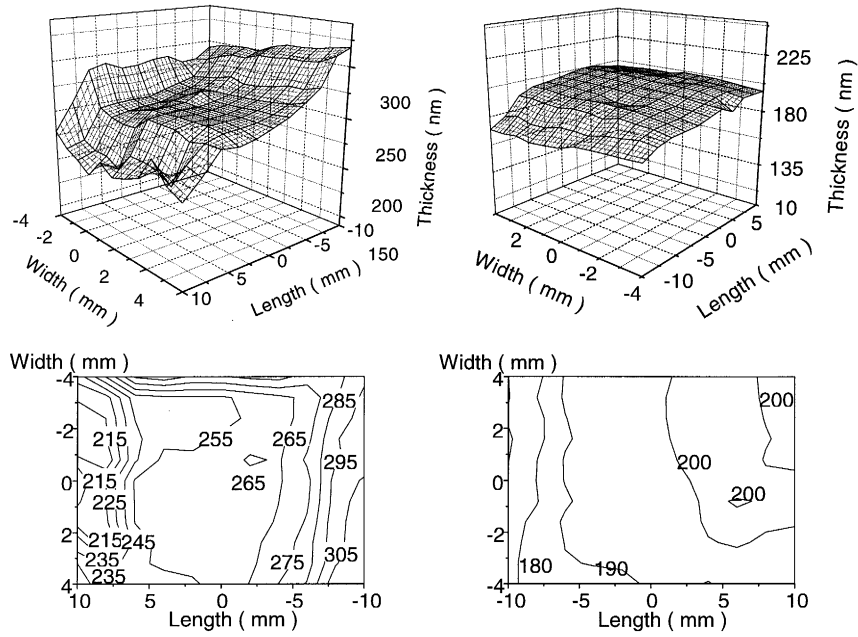
Fig. 4. Map surface and contour lines of sample S1 heat-treated for 12 h at 60 °C (left) and 500 °C (right).
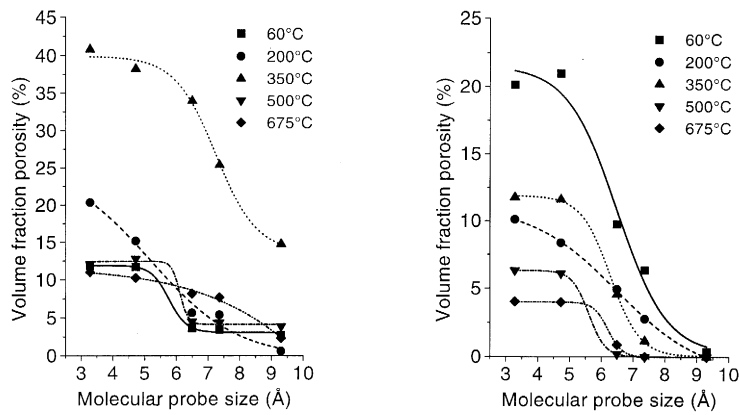
Fig. 5. Volume fraction porosity obtained by MPE at different temperatures of samples S1 (left) and S3 (right). The curves are obtained by a sigmoidal fitting of experimental data.
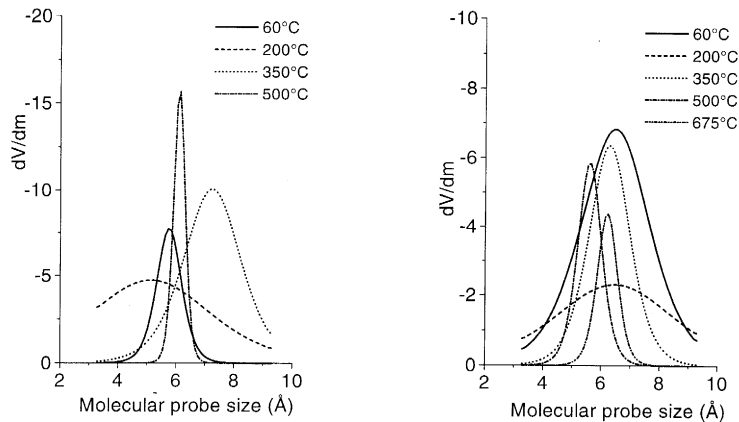
Fig. 6. Pore distribution of samples S1 (left) and S3 (right) obtained by differentiating curves of Fig. 5. The sizes are referred in all cases at each probe molecule to Van der Waals equivalent sphere diameter.

temperature than S1, leading to a lower porosity increase after the organics removal in the 200–350 °C temperature range.

Fig. 6 shows the pore size distribution obtained differentiating the sigmoidal curves of Fig. 5. Peak position, width and area are related to the mean pore size, root mean square deviation and total pore volume respectively. The S1 sample's pore volume (Fig. 6(a)) presents an increase between 60 and 350 °C caused by the pores getting rid of organic residues (peaks 1, 2 and 3 of the DTG). The maximum of pore distribution in the 60–200 °C shifts towards lower size values, indicating that adsorbed species remain in the smaller pores below 200 °C. When the S1 film is heat treated at 350 °C, the pores are void of organics. There seems to be an obvious size change related to the amount of organics covering pore walls. However, heat treatments above 350 °C lead to a decrease in the total porosity.

S3 porosity thermal evolution (Fig. 6(b)) differs from S1 behaviour. In this case the 60–350 °C increase in total pore volume is less important than in S1. This can be explained by the effect of sintering at low temperatures, that compensates the porosity increase due to elimination of organics. The maximum of pore distribution does not change between 60 and 200 °C, because there is no organics removal. Nevertheless between 200 and 350 °C the peak shifts to relatively lower size values and the peak area increases are in accordance with the elimination of organic locked in pore walls as explained by the DTG results. Between 350 and 675 °C the peak area decreases, the final pore distribution being very narrow. This is expected due to the film sintering. It is possible to detect some remaining porosity in heat-treated samples at the highest temperature.

4. Conclusions

Reflection ellipsometry has shown thickness uniformity of mullite-like amorphous dip-coated AISI 304. Thickness and refractive index evolution by heat treatment have also been determined to monitor the sintering. Sintering starts above 500 °C for silica alumina films deposited using TBA. Films deposited using $Al(NO_3)_3 \cdot 9H_2O$ begin to sinter at temperatures near 300 °C below those with TBA.

Molecular probe ellipsometry on films deposited over stainless steel is an adequate method to evaluate film microporosity, as well as a convenient alternative to other techniques. Porosity results are correlated with DTG experiments carried out on bulk gels. As it may be expected there is an important porosity decrease in heat-treated samples. However, remaining porosity is detected in samples treated at 675 °C.

Films deposited using $Al(NO_3)_3 9H_2O$ react with heat treatments in the same way as its bulk gel counterparts.

References

[1] O. de Sanctis, L. Gomez, N. Pelligri, C. Parodi, A. Marajofski and A. Duran, *J. Non-Cryst. Solids, 121* (1990) 338.

[2] M. Guglielmi, D. Festa, P.C. Innocenzi, P. Colombo and M. Gobain, *J. Non-Cryst. Solids, 147&148* (1992) 474.

[3] A.R. Di Giampaolo, M. Puerta, J. Lira and N. Ruiz, *J. Non-Cryst. Solids, 147&148* (1992) 474.

[4] M. Atik and M.A. Aegerter, *J. Non-Cryst. Solids, 147&148* (1992) 474.

[5] P. de Lima Neto, M. Atik, L.A. Avaca, M.A. Aegerter. *J. Sol–Gel Sci. Technol., 1* (1994) 177.

[6] K. Izumi, H. Tanaka, Y. Uchida, N. Tohge and T. Minami, *J. Non-Cryst. Solids, 147&148* (1992) 474.

[7] R. di Maggio, P. Scardi and A. Tomas, *Mater. Res. Soc. Symp., 180* (1990) 481.

[8] P. de Lima Neto, M. Atik, L.A. Avaca and M.A. Aegerter. *J. Sol–Gel Sci. Technol., 2* (1994) 529.

[9] E.M. Yeatman, M. Green, E.J.C. Dawnay, M.A. Fardad and F. Horowitz. *J. Sol–Gel Sci. Technol., 2* (1994) 711.

[10] M.A. Fardad, E.M. Yeatman, E.J.C. Dawnay, M. Green, and F. Horowitz, *J. Non-Cryst. Solids, 183* (1995) 260.

[11] J.C. Huling and G.L. Messing, *J. Non-Cryst. Solids 147&148* (1992) 213; F.L. MacCrackins, E. Pasaglia, R. Stromberg and H.L. Steiberg, *J. Res. Natl. Bur. Std., 67a* (1963) 363.

[12] J.C. Huling and G.L. Messing, *J. Non-Cryst. Solids 147&148* (1992) 213; F.L. Macrackins, E. Pasaglia, R. Stromberg and H.L. Steiberg, *J. Res. Natl. Bur. Std., 67a* (1963) 363.

[13] F.L. Macrackins, E. Pasaglia, R. Stromberg and H.L. Steiberg, *J. Res. Natl. Bur. Std., 67a* (1963) 363.

[14] L. Macrackins and J. Colson, *Computational Techniques for the use of the exact drude equations in reflection problems; The Symposium of the Ellipsometer and Its Use in The Measurements of Surfaces and Thin Films*, Washington, D.C. 1963, held under the auspices of the National Bureau of Standards, Miscellaneous Publications 256.

[15] D.E. Apsnes, *Thin Solid Films, 89* (1992) 249.